

## A Comparison Study of EOF Techniques: Analysis of Nonstationary Data with Periodic Statistics

KWANG-Y. KIM AND QIGANG WU

*Climate System Research Program, Texas A&M University, College Station, Texas*

(Manuscript received 2 December 1997, in final form 12 February 1998)

### ABSTRACT

Identification of independent physical/dynamical modes and corresponding principal component time series is an important aspect of climate studies for they serve as a tool for detecting and predicting climate changes. While there are a number of different eigen techniques their performance for identifying independent modes varies. Considered here are comparison tests of eight eigen techniques in identifying independent patterns from a dataset. A particular emphasis is given to cyclostationary processes such as deforming and moving patterns with cyclic statistics. Such processes are fairly common in climatology and geophysics. Two eigen techniques that are based on the cyclostationarity assumption—cyclostationary empirical orthogonal functions (EOFs) and periodically extended EOFs—perform better in identifying moving and deforming patterns than techniques based on the stationarity assumption. Application to a tropical Pacific surface temperature field indicates that the first dominant pattern and the corresponding principal component (PC) time series are consistent among different techniques. The second mode and the PC time series, however, are not very consistent from one another with hints of significant modal mixing and splitting in some of derived patterns. There also is a detailed difference of intraannual scale between PC time series of a stationary technique and those of a cyclostationary one. This may bear an important implication on the predictability of El Niño. Clearly there is a choice of eigen technique for improved predictability.

### 1. Introduction

A primary goal of empirical orthogonal function (EOF) analysis is to identify and extract from a dataset physically and dynamically independent patterns also called normal modes (Schnur et al. 1993; Dunkerton 1993; Braconnot and Frankignoul 1993; Zwiers 1993; Xu 1993; Montroy 1997; to name only a few studies). These independent “modes” provide important clues as to the physics and dynamics of the system to be studied. Another important but poorly recognized goal of EOF analysis is to represent natural variability, or background fluctuations, in terms of a set of orthogonal functions. Such is called a basis set. In meteorology, North and Cahalan (1981) were probably the first to recognize this and used the EOF expansion of spatial covariance functions in a study of sampling errors.

One essential application of EOFs in climate studies is in the areas of prediction, estimation, and detection of climatic changes. They are collectively called the linear estimation study. A statistical prediction exercise typically consists of identifying physical and/or dynam-

ical modes and evaluating their future values. Since the success of prediction, in a large part, depends on the faithful extraction of meaningful modes, often elaborate EOF techniques are employed in such studies (e.g., Graham et al. 1987a,b; Xu and von Storch 1990; Blumenthal 1991).

In a detection study, background noise is decomposed into EOFs, which serve as a set of orthogonal basis functions. Then a signal, decomposed into the same EOFs, is compared with the noise mode by mode. Modes with higher signal-to-noise ratio certainly are more beneficial and are weighted accordingly for the signal detection (Hasselmann 1993; Santer et al. 1994; North et al. 1995; North and Kim 1995; Hegerl et al. 1996). This EOF representation of background noise, or natural variability, is extremely useful. EOFs are constructed such that they are independent, at least computationally, of each other. Thus, each principal component (PC) time series represents an independent random variable and the use of joint probability distribution function can be avoided in a statistical test. This EOF representation was proven to be useful also in many estimation studies (Shen et al. 1994; Kim et al. 1996b; Kim 1997).

It is rather obvious that accuracy of EOFs and eigenvalues are important in linear estimation studies. An immediate question, then, is which among a number of

---

*Corresponding author address:* Dr. Kwang-Y. Kim, Climate System Research Program, College of Geosciences and Maritime Studies, Texas A&M University, College Station, TX 77843-3150.  
E-mail: kykim@csr.tamu.edu

EOF techniques is best for a given dataset and purpose. Such a question can only be answered case by case because each technique has its own strength and weakness. The property of each technique in comparison with others has not yet been fully investigated through comparison studies and has only naively been perceived. This study examines eight different EOF techniques via a suite of experiments that are schematic but are easy to understand. It should be pointed out that exhaustive comparison tests are too big to be carried out here. One important factor considered in this comparison study is cyclostationarity.

There is an increasing tendency to take into account the cyclostationarity of data in climate studies (Blumenthal 1991; Penland and Magorian 1993; von Storch et al. 1995; Chen et al. 1995; Davey et al. 1996). See Kim et al. (1996a) and Kim and North (1997) for the definition of cyclostationary or periodically correlated processes. Such a tendency is natural since many geophysical and climatic processes are approximately cyclostationary. Strong seasonality in the statistics of surface temperature and surface precipitation, for instance, is rather obvious. Some EOF techniques are tuned to the analysis of stationary data while others are geared more toward the cyclostationary analysis. Some techniques inevitably introduce inaccuracies into the computation of EOFs. Then, the question of aptitude and accuracy of a certain technique emerges immediately. Bear in mind that the tests here are limited in scope to the analysis of data with periodic statistics.

Section 2 has a brief description of EOF techniques employed in this study. Detailed description of the techniques is repressed and is referred to more pertinent publications. Description of three tests appears in section 3 followed by the test results in the next section. In section 5, a limited sensitivity test is conducted for the cyclostationary EOF technique that yields the best result in the previous section. Then, each technique is compared to others as applied to tropical surface temperature (ST) for major patterns of El Niño. Then, a brief summary and concluding remarks follow.

## 2. Description of employed eigen techniques

Eight different eigen techniques have been employed in this study. They are 1) regular EOF, 2) rotated EOF (REOF), 3) complex EOF (CEOF), 4) extended EOF (EXEOF), 5) periodically extended EOF (PXEOF), 6) principal oscillation pattern (POP), 7) cyclostationary POP (CSPOP), and 8) cyclostationary EOF (CSEOF) techniques. A common aspect of these techniques is that they find eigenfunctions and eigenvalues of a matrix. In most techniques, this matrix is referred to as a covariance matrix,  $\{C_{ij}\}$ , where  $i$  and  $j$  are data points. A covariance matrix is derived from the spatial covariance function of a given dataset or its variant. In the POP and CSPOP techniques, it is called the system matrix. It is derived from lagged spatial covariance functions.

How such a matrix, either covariance matrix or system matrix, is derived from a dataset deviates from one method to another and it entails the difference between different techniques.

In a regular EOF analysis, a covariance matrix is simply the spatial covariance function of data at the specified grid points:

$$C_{ij} = \langle T_i T_j \rangle, \quad (1)$$

where  $T_i = T(\hat{\mathbf{r}}_i, t)$  is the value of data at a point  $\hat{\mathbf{r}}_i$  and  $\langle \cdot \rangle$  implies ensemble averaging. This analysis may be useful in identifying stationary patterns.

A rotated EOF analysis employed in this study is based on the varimax rotation (Richman 1986; Barnston and Livezey 1987; Cheng et al. 1995; Montroy 1997). In essence, EOF patterns,  $\hat{\mathbf{p}}_k(\hat{\mathbf{r}})$ ,  $k = 1, \dots, K$ , are rotated such that the so-called ‘‘simplicity’’ functional  $S$  is minimized as a result of rotation:

$$S(\hat{\mathbf{q}}_1, \hat{\mathbf{q}}_2, \dots, \hat{\mathbf{q}}_K) = \sum_{k=1}^K f(\hat{\mathbf{q}}_k), \quad (2)$$

where

$$f(\hat{\mathbf{q}}) = \frac{1}{m} \sum_{i=1}^m \left[ \left( \frac{\hat{\mathbf{q}}(\hat{\mathbf{r}}_i)}{s_i} \right)^2 \right]^2 - \frac{1}{m^2} \left[ \sum_{i=1}^m \left( \frac{\hat{\mathbf{q}}(\hat{\mathbf{r}}_i)}{s_i} \right)^2 \right]^2. \quad (3)$$

Here,  $\hat{\mathbf{q}}_k(\hat{\mathbf{r}})$ ,  $k = 1, \dots, K$ , are rotated EOFs and  $s_i$  is the standard deviation at point  $\hat{\mathbf{r}}_i$ . The varimax rotation is an orthogonal transformation and yields a set of orthogonal eigenfunctions. The technique is known to yield more stable spatial patterns in general (Richman 1986; Montroy 1997).

In a complex EOF analysis (Wallace and Dickinson 1972; Horel 1984; Barnett 1983, 1985) real dataset is extended into a complex variable the imaginary part of which is Hilbert transform of the real part:

$$\tilde{T}(\hat{\mathbf{r}}, t) = T(\hat{\mathbf{r}}, t) + \mathcal{H}(T(\hat{\mathbf{r}}, t)), \quad (4)$$

where

$$\mathcal{H}(T(\hat{\mathbf{r}}, t)) = \sum_{\omega} c_H(\hat{\mathbf{r}}, \omega) e^{-2\pi i \omega t} \quad (5)$$

and

$$c_H(\hat{\mathbf{r}}, \omega) = \begin{cases} ic(\hat{\mathbf{r}}, \omega) & \text{for } \omega \geq 0 \\ -ic(\hat{\mathbf{r}}, \omega) & \text{for } \omega < 0. \end{cases} \quad (6)$$

The  $c(\hat{\mathbf{r}}, \omega)$  are the expansion coefficients of  $T(\hat{\mathbf{r}}, t)$ ; that is,

$$T(\hat{\mathbf{r}}, t) = \sum_{\omega} c(\hat{\mathbf{r}}, \omega) e^{-2\pi i \omega t}, \quad (7)$$

where  $\omega$  is the natural frequency. A covariance matrix is obtained from a complex variable (4). Since the imaginary part (Hilbert transform) represents the phase shift by a quarter of a period, complex EOFs may be suited for identifying moving patterns.

The extended EOF analysis (Weare and Nasstrom 1982) is mathematically equivalent to the multichannel

singular spectral analysis (Plaut and Vautard 1994). In both techniques, a covariance matrix is augmented by time-lagged covariance functions. That is,

$$\mathbf{C} = \begin{pmatrix} \mathbf{C}(0) & \mathbf{C}(1) & \mathbf{C}(l) \\ \mathbf{C}(1) & \mathbf{C}(0) & \mathbf{C}(l-1) \\ & & \ddots \\ \mathbf{C}(l) & \mathbf{C}(l-1) & \mathbf{C}(0) \end{pmatrix}, \quad (8)$$

where the lag- $l$  spatial covariance matrix is

$$\mathbf{C}(l) = \langle T(\hat{\mathbf{r}}, t)T(\hat{\mathbf{r}}', t + l) \rangle. \quad (9)$$

Here  $\hat{\mathbf{r}}$  and  $\hat{\mathbf{r}}'$  represent two different locations and the elements of  $\mathbf{C}(l)$  are defined as in (1). The resulting covariance matrix is equivalent to considering a new variable,

$$\tilde{T}(\hat{\mathbf{r}}, t) = \{T(\hat{\mathbf{r}}, t), T(\hat{\mathbf{r}}, t + 1), \dots, T(\hat{\mathbf{r}}, t + l)\}, \quad (10)$$

which consists of time-lagged data. This technique is intended for space-time (moving) patterns of data by taking both the spatial and temporal correlations into account (Lau and Chan 1985; Graham et al. 1987a,b).

A variant of the extended EOF technique is the following:

$$\mathbf{C} = \begin{pmatrix} \mathbf{C}_{1,1} & \mathbf{C}_{1,2} & \mathbf{C}_{1,l} \\ \mathbf{C}_{2,1} & \mathbf{C}_{2,2} & \mathbf{C}_{2,l} \\ & & \ddots \\ \mathbf{C}_{l,1} & \mathbf{C}_{l,2} & \mathbf{C}_{l,l} \end{pmatrix}, \quad (11)$$

where

$$\mathbf{C}_{jk} = \langle T(\hat{\mathbf{r}}, j + lt)T(\hat{\mathbf{r}}', k + lt) \rangle, \quad j, k = 1, \dots, l, \quad (12)$$

the ensemble being taken for  $t$  and  $l$  is the period. Let us call it a periodically extended EOF technique. The covariance matrix (11) is derived by dividing data into  $l$  periodic segments and treating them as different variables; that is,

$$\tilde{T}(\hat{\mathbf{r}}, t) = \{T(\hat{\mathbf{r}}, 1 + lt), T(\hat{\mathbf{r}}, 2 + lt), \dots, T(\hat{\mathbf{r}}, l + lt)\}. \quad (13)$$

The technique is a sensible generalization for a variable with periodic statistics and it will be useful for identifying any periodic patterns.

POP and CSPOP analyses are somewhat different from other EOF techniques and are oriented more toward the modeling of dynamical systems. Since the technique was first introduced by Hasselmann (1988), POP analysis have frequently been used in climate studies (e.g., Latif and Flügel 1991; Latif et al. 1993; Bürger 1993; Barnett et al. 1993). The POP technique identifies essentially a multivariate autoregressive (AR) model:

$$T(\hat{\mathbf{r}}, t + 1) = \mathbf{A}T(\hat{\mathbf{r}}, t) + \epsilon(\hat{\mathbf{r}}, t), \quad (14)$$

where the system matrix  $\mathbf{A}$  is

$$\mathbf{A} = \mathbf{C}(1)\mathbf{C}(0)^{-1} \quad (15)$$

and  $\mathbf{C}(0)$  and  $\mathbf{C}(1)$  covariance matrices at lag 0 and 1, respectively. Dominant spatial patterns, called POPs, are obtained as eigenfunctions of the system matrix  $\mathbf{A}$ . The system matrix is not symmetric in general and complex eigenvalues and conjugate pairs of complex eigenfunctions should be expected. A complex eigenfunction may represent an oscillating pattern.

CSPOP is a generalization of POP for cyclostationarity of data (Blumenthal 1991; von Storch et al. 1995). A cyclostationary AR model may be written as

$$T(\hat{\mathbf{r}}, t, \tau + 1) = \mathbf{A}(\tau)T(\hat{\mathbf{r}}, t, \tau) + \epsilon(\hat{\mathbf{r}}, t, \tau), \quad (16)$$

where  $t$  represents a cycle and  $\tau$  is nested time within a cycle. Note that the system matrix depends upon the nested time  $\tau$  and is assumed periodic; that is,

$$\mathbf{A}(\tau + l) = \mathbf{A}(\tau). \quad (17)$$

Cyclostationary POPs are obtained as eigenfunctions of the matrix

$$\mathbf{B}(\tau) = \mathbf{A}(\tau + l - 1)\mathbf{A}(\tau + l - 2) \cdots \mathbf{A}(\tau). \quad (18)$$

It can be proved that the eigenvalues of  $\mathbf{B}(\tau)$  are independent of  $\tau$ . Eigenfunctions, however, are dependent upon  $\tau$ .

As in CSPOP analysis, CSEOFs are also characterized by two temporal scales. This, of course, is in consideration of the periodic statistics of cyclostationary processes. There are two computational methods—one based on Bloch's theorem (Kim et al. 1996a) and the other based on the assumption of harmonizable cyclostationary processes (Kim and North 1997). The latter method yields approximate CSEOFs but is much more efficient computationally. The essence of the method is to write a given data in the form

$$T(\hat{\mathbf{r}}, t) = \sum_{k=0}^{d-1} a_k(\hat{\mathbf{r}}, t)e^{2\pi ikt/d}, \quad (19)$$

where  $d$  is the nested period of a cyclostationary process. We shall call  $a_k(\hat{\mathbf{r}}, t)$  coefficient time series. A new variable is constructed by juxtaposing coefficient time series as

$$\tilde{T}(\hat{\mathbf{r}}, t) = \{a_1(\hat{\mathbf{r}}, t), a_2(\hat{\mathbf{r}}, t), \dots, a_d(\hat{\mathbf{r}}, t)\}. \quad (20)$$

Then, CSEOFs are obtained as eigenfunctions of the covariance matrix of this new variable.

### 3. Test procedures

Described here are three different datasets that are used to test these EOF techniques. The first dataset consists of two stationary patterns of an anomaly with fixed forms on top of a noise field (Fig. 1). Each mound is forced by an autoregressive order-1 process (hereafter AR-1) so that its strength changes in time. The dataset consists of  $21 \times 15$  arrays of length 564 points. The two patterns are stationary in the sense that the applied

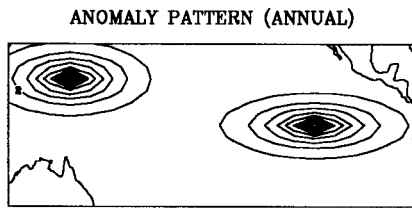


FIG. 1. Two physical modes in the dataset of experiment 1. Each pattern is fixed in shape but changes in amplitude in time scaled by an AR-1 random forcing that is stationary. The percent variance explained by each mode (from left to right) is 14% and 86%, respectively.

forcing time series are stationary and that its shape does not change in time. Their percent variances are 14% and 86%, respectively. The variance of each mode represents the variance of the driving force (i.e., PC time series) after each pattern is normalized in magnitude. The second dataset consists of two patterns of anomaly that are changing in shape periodically with time on top of a noise field (Fig. 2). The random forcings that drive these mounds are stationary but the anomaly patterns are not stationary because their shapes change in time. Their percent variances are 7% and 93%, respectively. The third dataset represents two moving patterns of anomaly on top of a noise field (Fig. 3). The two patterns are periodic and move at different speeds. The forcing time series are stationary. Again, the anomaly patterns are not stationary because their positions change in time. Their percent variances are 14% and 86%, respectively.

The first dataset represents a stationary process in space and time. Most EOF techniques are supposed to isolate the independent patterns of this stationary dataset. This particular experiment, seemingly obvious, was included to examine if EOF techniques designed for cyclostationary analysis, such as CSPOP and CSEOF, can handle this trivial case correctly.

The latter two datasets represent nonstationary processes with the patterns and strength of anomalies change periodically. For convenience let us assert that the time step is one month and the periodicity is one year. They are particular examples of cyclostationary processes since the statistics of the datasets are approximately cyclic both in space and time. A design concept of these experiments was that often moving and deforming physical and dynamical patterns are of our interest in geophysics and climatology. A typical example is the ST patterns associated with El Niño. More general, nonstationary datasets are beyond the scope of this study and none of the EOF techniques addressed here qualifies for them.

Finally, it is emphasized that the background noise field is very weak in all the synthetic datasets (typically less than 1% of total variability). Also, the record is reasonably long. Such a design consideration is to separate the issue of the accuracy of eigen techniques in dealing with cyclostationary datasets from the issue of sampling error. As will be evident in the test results

sampling error is almost completely suppressed. Also, the anomalies are purposely detached from the boundary of the domain so that the domain shape in conjunction with the orthogonality requirement does not have any impact on the topology of resulting patterns (Buell 1975, 1979; Richman 1986). Again, test results indicate that the derived physical patterns are almost free of any impact from the shape of the domain.

#### 4. Test results

Discussed here are the test results of the experiments. The results are in the form of pattern correlation and temporal correlation of the derived EOF patterns and the corresponding PC time series with those of the two physical modes explained in the previous section. We will use the term “physical” modes in contrast to “computational” modes. There is no universally accepted criterion for a good match but let us define it in terms of correlation greater than 0.9 and modal mixing (correlation of the second best match) less than 0.1 in both time and space. In the case of complex EOF analysis, pattern correlations were computed using both real and imaginary patterns. Then, the larger of the two were taken. POPs and cyclostationary POPs are also complex patterns in general. In this study, all the meaningful POPs and CSPOPs with maximum correlations with the physical modes are real and therefore pose no complication in computing pattern correlations. Further, monthly POP patterns are lagged such that the maximum pattern correlation is achieved between physical modes and POPs in the cyclostationary POP analysis. Then, corresponding PC time series are computed.

##### a. Experiment 1

For a stationary anomaly field (Fig. 1) EOF, REOF, EXEOF, PXEOF, and CSEOF techniques identify the two modes in the dataset correctly. Both the pattern and temporal correlations with the physical modes are high for these techniques (Table 1). Surprisingly enough other techniques have a varying degree of difficulty in identifying these simple modes. One common problem clearly discernable from the derived patterns in the latter techniques is that the two modes are not well separated (e.g., see Fig. 4).

The modal mixing in CEOFs can be explained in terms of the cross-correlation between the PC time series and their Hilbert transformations. Note that the PC time series are uncorrelated with each other and so are their Hilbert transformations. Note also that regular EOF analysis for the transformed dataset and the original dataset results in identical patterns. While each Hilbert transformation is uncorrelated with its original time series, the former is not uncorrelated with other PC time series and vice versa. This causes cross-covariance between the original PC time series and their Hilbert transformations and modal mixing as a result. This simple

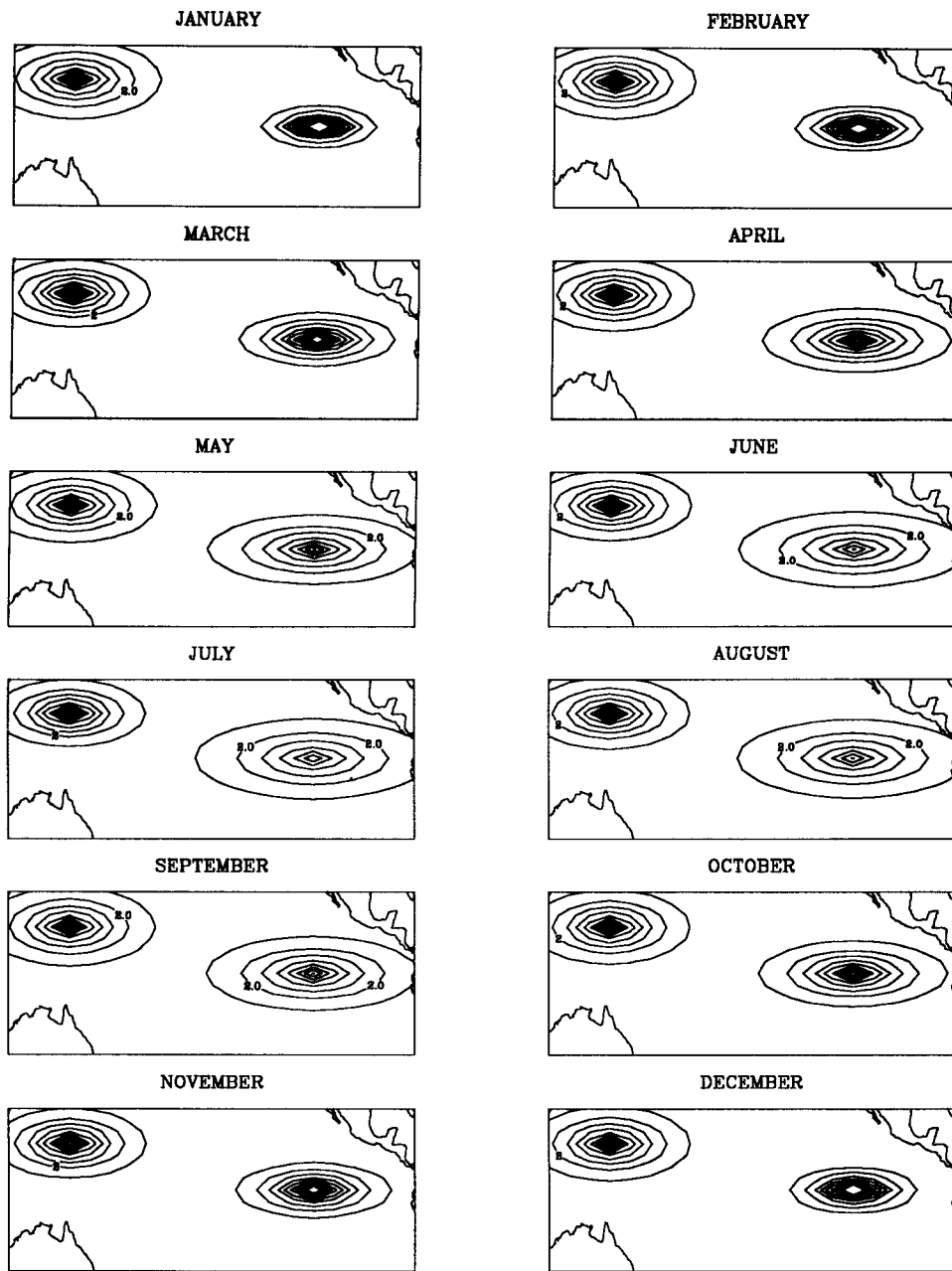


FIG. 2. Two physical modes in the dataset of experiment 2. Each pattern changes in shape periodically in time. The amplitude of each pattern also changes in time scaled by a random noise that is stationary. The percent variance explained by each mode (from left to right) is 7% and 93%, respectively.

test indicates that modal mixing is inevitable in CEOF analysis unless each mode is first separated somehow prior to the analysis. If two modes have very different frequencies they can be separated by simple filtering, which is frequently done in practice.

While POP and CSPOP techniques in essence find a multivariate, AR-1 model that best fits a given dataset [see (14) and (16)], there is no a priori justification that such a model is most suitable for identifying patterns

in the dataset. This statement does not imply that the methodologies are not useful. There certainly are ample examples that prove the utility of the techniques. Note that this AR-1 representation naturally comes from the discretization of a first-order Markov process. The present dataset simply does not conform to the first-order Markov process. It is emphasized that fitting a prescribed model to a dataset can result in spurious modes or modal mixing.

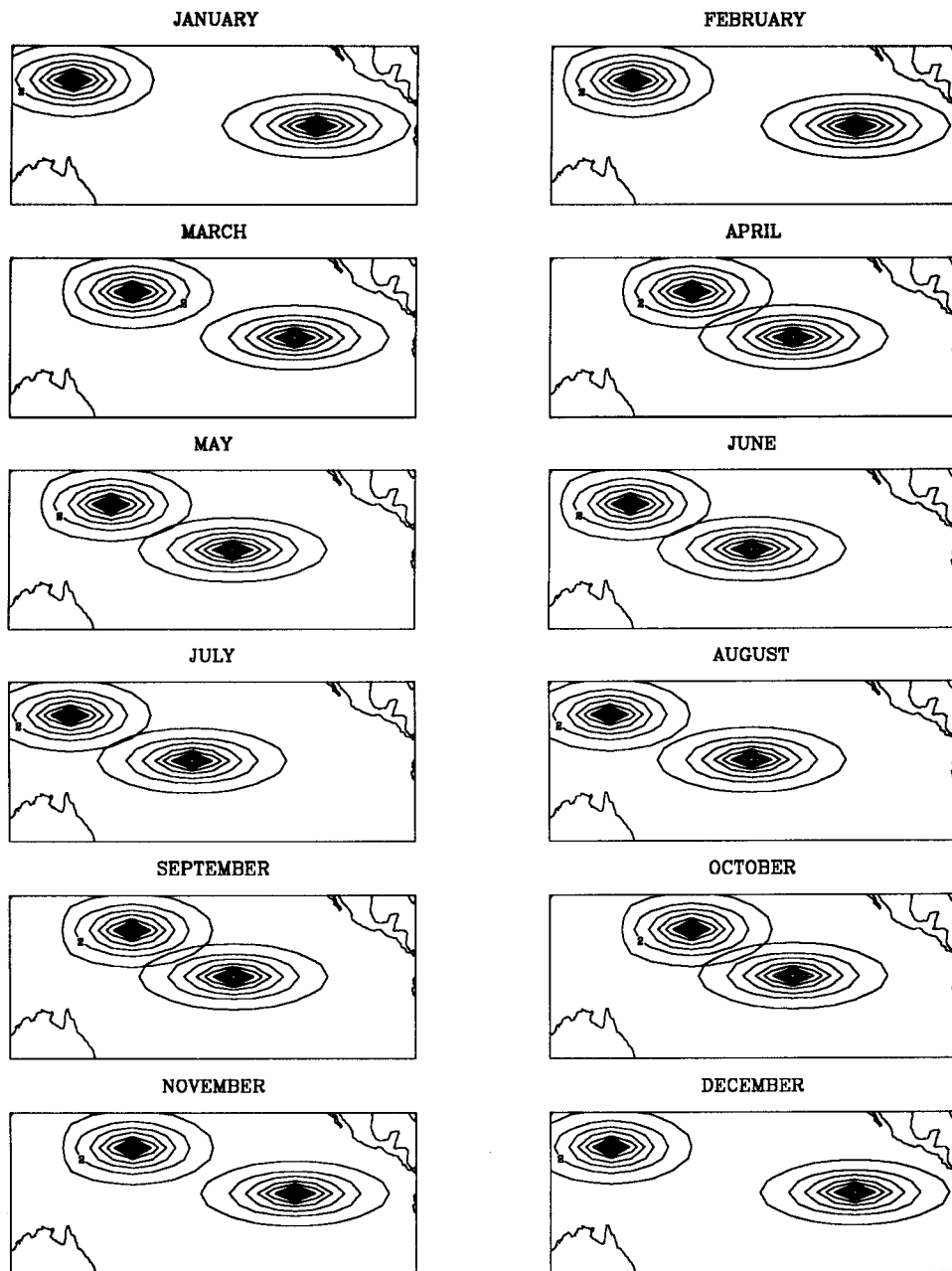


FIG. 3. Two physical modes in the dataset of experiment 3. Each pattern moves periodically in time. The amplitude of each mound changes in time scaled by a random forcing that is stationary. The percent variance explained by each mode (from left to right) is 14% and 86%, respectively.

In the PXEOF technique, given data are periodically divided into a number of segments each of which is a new variable [see (13)]. If the given data are truly stationary, the statistics of these new variables should be identical. Then, the resulting covariance matrix in (11) should be periodic and each block denoted as  $\mathbf{C}_{jk}$  should be identical. Thus, the PXEOFs should be identical for each time section. Such is the case for the present exercise.

#### b. Experiment 2

When the physical modes change in shape with time (Fig. 2), all of the eigen techniques except for PXEOF and CSEOF exhibit some difficulty in identifying correct evolving patterns. One common problem is the mixing of modes. Derived patterns of CEOF, POP, and CSPOP clearly show signs of modal mixing (see also pattern and temporal correlations in Table 2). The mechanism of mixing is similar to the previous experiment.

TABLE 1. Spatial and temporal correlations of the derived EOF patterns and the corresponding principal component time series with those of the two physical modes (modes 1 and 2) from experiment 1. Each block consists of two lines of entries: best pattern correlation and cross correlation with mode numbers in parenthesis (first line), and best temporal correlation and cross correlation (second line). The acronyms stand for EOF for regular empirical orthogonal function, REOF for rotated EOF, CEOF for complex EOF, EXEOF for extended EOF, PXEOF for periodically extended EOF, POP for principal oscillation pattern, CSPOP for cyclostationary POP, and CSEOF for cyclostationary EOF.

Method	Mode 1 ( $\sigma^2 = 1200$ )		Mode 2 ( $\sigma^2 = 181$ )	
	EOF	1.00 (1)	0.01 (2)	1.00 (2)
	1.00	0.01	1.00	0.01
REOF	1.00 (1)	0.01 (2)	1.00 (2)	0.01 (1)
	1.00	0.02	1.00	0.03
CEOF	1.00 (1)	0.02 (2)	1.00 (2)	0.01 (1)
	1.00	0.01	0.86	0.01
EXEOF	1.00 (1)	0.00 (2)	1.00 (2)	0.01 (1)
	0.95	0.05	0.94	0.04
PXEOF	1.00 (1)	0.01 (2)	0.99 (2)	0.00 (1)
	1.00	0.01	1.00	0.00
POP	1.00 (1)	0.75 (2)	0.65 (2)	0.10 (1)
	1.00	0.95	0.32	0.03
CSPOP	0.98 (1)	0.15 (3)	0.31 (3)	0.20 (1)
	1.00	0.19	0.13	0.07
CSEOF	1.00 (1)	0.01 (2)	1.00 (2)	0.00 (1)
	0.99	0.00	0.99	0.00

Another common problem is the splitting of modes. Eigen techniques based on the stationarity assumption are not able to pick up evolving patterns. The only alternative is to split the evolving patterns into a series of orthogonal patterns that do not change in time. For example, modes 2 and 4 of Fig. 5 are a stationary representation of the evolving physical mode. This modal splitting is a typical problem for all eigen techniques based on the stationarity assumption including the REOF technique. It is rather obvious that actual modes in Fig. 2 cannot be obtained by rotating EOF patterns shown in Fig. 5.

This also implies that each EOF pattern does not have an accurate temporal structure. As a consequence PC time series may be erroneous. For example, the first two EXEOF patterns that have maximum resemblance with the physical modes do not change during the stipulated cycle (12 months) in contrast to the actual modes in Fig. 2. Inaccurate temporal structure of a spatial pattern should be reflected in the corresponding PC time series.

Both the CSEOF and PXEOF techniques do a fairly good job in reproducing the evolving patterns. Both the pattern and temporal correlations are good (Table 2). It is of no coincidence that CSEOFs look very similar to the actual modes. This technique is designed for cyclostationary processes. In the PXEOF technique, given data are periodically divided into a number of segments each of which is a new variable [see (13)]. For instance,

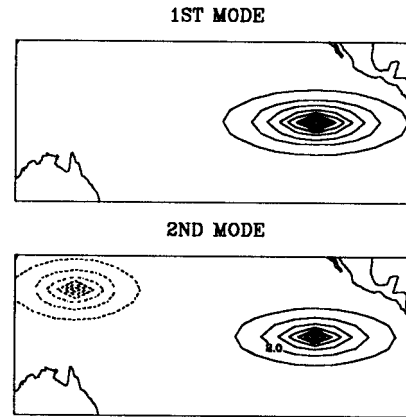


FIG. 4. Two POP patterns with maximum correlations with the physical modes (experiment 1). The two physical modes were not satisfactorily separated. The dashed lines represent negative contours.

each month is considered a different variable in a monthly observational data. This idea seems useful for analyzing cyclostationary datasets. Indeed, the evolution of the EOF patterns is similar to those of Fig. 2 (see also Table 2).

### c. Experiment 3

The third experiment is for moving anomaly patterns shown in Fig. 3. All the techniques except for PXEOF and CSEOF suffer from inaccuracies. Pattern correlations are generally poorer than in experiment 2 as a result of moving patterns. Both the CSEOF and PXEOF techniques do a fairly good job in reproducing the mov-

TABLE 2. Spatial and temporal correlations of the derived EOF patterns and the corresponding principal component time series with those of the two physical modes (modes 1 and 2) from experiment 2. The table entries and the acronyms are the same as in Table 1.

Method	Mode 1 ( $\sigma^2 = 294$ )		Mode 2 ( $\sigma^2 = 21$ )	
	EOF	0.89 (1)	0.02 (3)	0.99 (3)
	0.78	0.04	0.99	0.01
REOF	0.67 (2)	0.02 (3)	1.00 (3)	0.01 (2)
	1.00	0.03	0.99	0.04
CEOF	0.89 (1)	0.09 (3)	0.97 (3)	0.03 (1)
	0.78	0.08	0.71	0.01
EXEOF	0.93 (1)	0.00 (4)	0.99 (2)	0.02 (1)
	0.95	0.05	0.94	0.01
PXEOF	1.00 (1)	0.01 (2)	0.99 (2)	0.01 (1)
	1.00	0.09	0.99	0.05
POP	0.93 (1)	0.00 (7)	0.69 (7)	0.07 (1)
	0.83	0.03	0.85	0.01
CSPOP	0.71 (3)	0.33 (2)	0.79 (2)	0.05 (3)
	0.63	0.47	0.26	0.02
CSEOF	1.00 (1)	0.01 (2)	0.99 (2)	0.01 (1)
	1.00	0.01	1.00	0.04

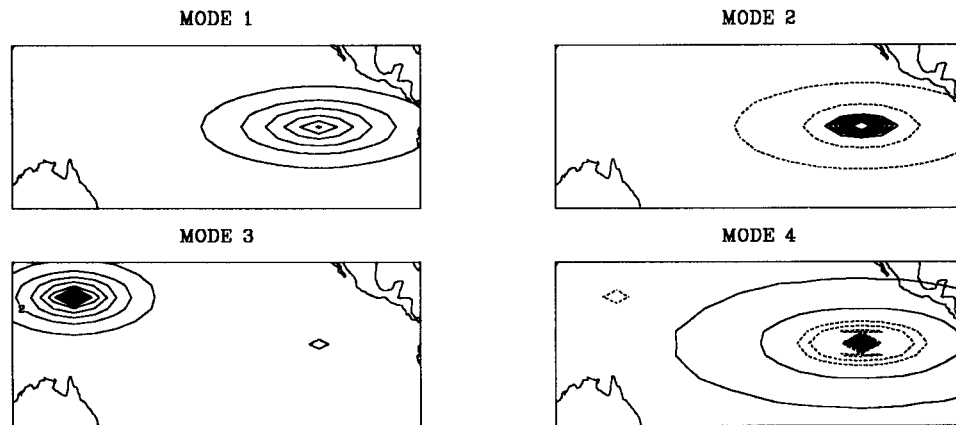


FIG. 5. Four EOF patterns (experiment 2). The second and fourth modes represent the variance splitting of the time evolving physical mode.

ing patterns (figures not shown). Pattern and temporal correlations for these techniques are good (Table 3). Again, one of common problems is modal mixing, which is apparent in many derived EOF patterns. Patterns of CEOF, POP, and CSPOP clearly show signs of modal mixing (see also Table 3).

Another common problem is mode splitting. Evolving patterns are split into a series of stationary patterns. This splitting is well demonstrated in the eigenvalues. More than two modes have significant variance ( $>10\%$ ) in all the eigen techniques based on the stationarity assumption. A stationary representation of moving patterns appears in the form of dipoles and elongated modes in the direction of motion (Fig. 6). The rotation of the EOFs indeed simplifies the patterns and the rotated EOFs do

not have notable dipole and elongated structures (Fig. 7). The REOF technique, on the other hand, divides a moving pattern into a series of stationary patterns, which obviously is a stationary representation of moving patterns.

### 5. Sensitivity of cyclostationary EOFs

As shown in the previous section the CSEOF technique performs best in identifying moving and deforming patterns with cyclic statistics. It is, then, legitimate to ask how sensitive CSEOFs and the associated PC time series are. Considered here is a Monte Carlo test of the sensitivity of CSEOFs to the length of records and the background noise level. Note that background noise implies uninteresting fluctuations of little or no physical origin. Also record length is an important source of sampling error.

For the test datasets of deforming and moving patterns similar to those in the experiments 2 and 3 above were created. Each dataset is  $21 \times 15$  in lateral extent and is 600 points long in time. The test employs seven different levels of background noise. The standard deviations of the employed background noise at each grid point are 0.01, 0.05, 0.1, 0.2, 0.5, 1.0, and 2.0, respectively. Background noise at each station is assumed to be random with a Gaussian distribution with zero mean and a prescribed standard deviation. It is cautioned that such an assumption is introduced merely to simplify the experiment but may not be accurate. For each level of background noise 10 different realizations were generated using a random number generator. Then, CSEOFs were extracted from each realization employing five different sampling lengths: 10, 20, 30, 40, and 50 yr, respectively. The sensitivity is measured in terms of the magnitude of the eigenvalues, the PC time series correlations, and the pattern correlations of the first two modes with those of an error-free dataset. The standard deviations of these quantities were also computed from 10 realizations.

TABLE 3. Spatial and temporal correlations of the derived EOF patterns and the corresponding principal component time series with those of the two physical modes (modes 1 and 2) from experiment 3. The table entries and the acronyms are the same as in Table 1.

Method	Mode 1 ( $\sigma^2 = 1190$ )		Mode 2 ( $\sigma^2 = 183$ )	
	EOF	0.83 (2) 0.96	0.01 (4) 0.06	0.83 (4) 0.98
REOF	0.72 (2) 0.92	0.04 (6) 0.09	0.58 (6) 0.72	0.00 (2) 0.03
CEOFF	0.83 (2) 0.96	0.00 (4) 0.04	0.83 (4) 0.83	0.08 (2) 0.01
EXEOF	0.83 (1) 0.95	0.00 (6) 0.01	0.83 (6) 0.94	0.08 (1) 0.05
PXEOF	0.99 (1) 1.00	0.01 (2) 0.02	0.97 (2) 1.00	0.06 (1) 0.01
POP	0.83 (1) 0.98	0.56 (2) 0.89	0.58 (2) 0.38	0.14 (1) 0.03
CSPOP	0.27 (1) 0.32		0.01 (1) 0.00	
CSEOF	0.99 (1) 1.00	0.01 (2) 0.02	0.97 (2) 1.00	0.08 (1) 0.01

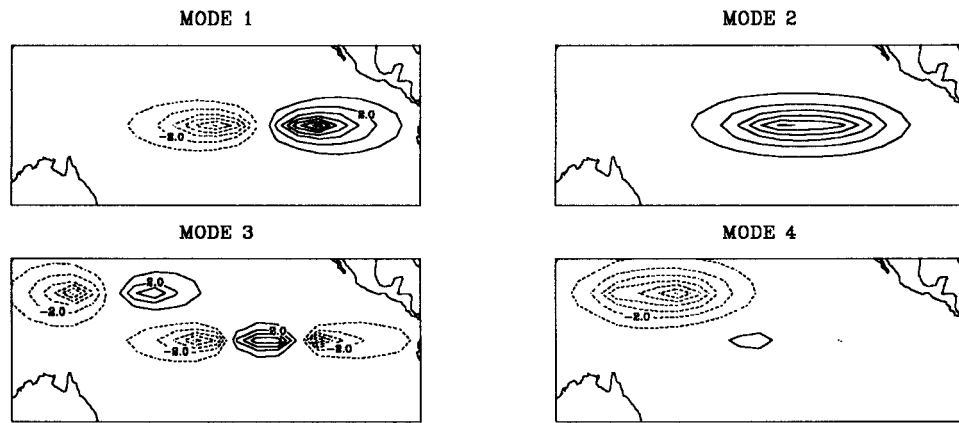


FIG. 6. Four EOF patterns (experiment 3). The first and third modes have dipole structures. The second and fourth modes are elongated compared with the exact physical modes. Derived patterns often have such structures when physical modes are moving.

Figure 8 shows the first two eigenvalues and the sum of them for the first datasets with deforming patterns. The exact eigenvalues are 1.02 and 0.806 for the two modes, respectively. The eigenvalues were reproduced reasonably until the background noise level reaches 0.2 (about 20% of the first exact eigenvalue). Beyond this level of background noise eigenvalues were seriously overestimated. For example, errors are 25% and 31% for the first two eigenvalues for panel (e) in Fig. 8. Estimates of eigenvalues also deteriorate as sampling length decreases as should be expected. For example, at the background noise level of 0.2 [panel (d)] the standard deviation of estimation increases from 0% to 50% and 61% for the first two eigenvalues, respectively, when the sampling length decreases from 50 to 10 years.

Figure 9 shows the cross-pattern correlations between the two exact modes and two estimates. As expected, extracted patterns become progressively dissimilar from the exact modes as background noise increases and the record length decreases. For panel (e), pattern correlations are 0.90 and 0.88 for the first two modes, respec-

tively, when the estimation is based on 50-yr record. For a 10-yr record, the respective pattern correlations are  $0.56 \pm 0.10$  and  $0.43 \pm 0.13$ . Note also that cross-pattern correlations are rather sensitive to the record length. Even for small background noise cross-pattern correlations are significant, reaching 0.53 and 0.54 for a 10-yr record [panel (a)]. This nonzero cross correlation indicates modal mixing. The degree of modal mixing depends crucially on the ratio of sampling error (in terms of the magnitude and the record length) to the separation of two eigenvalues (North 1984). Cross pattern correlations are reasonable if the level of background noise does not exceed 50% of modal variances (eigenvalues) for a sufficiently long record.

Cross-temporal correlations show similar trends to those of the pattern correlations (see Fig. 10). As in the case of the pattern correlations similarity between the exact PC time series and their estimates quickly deteriorates as the record length decreases. For instance, temporal correlations decrease from 1.00 to 0.77 and 0.53, respectively, for the two modes and cross-corre-

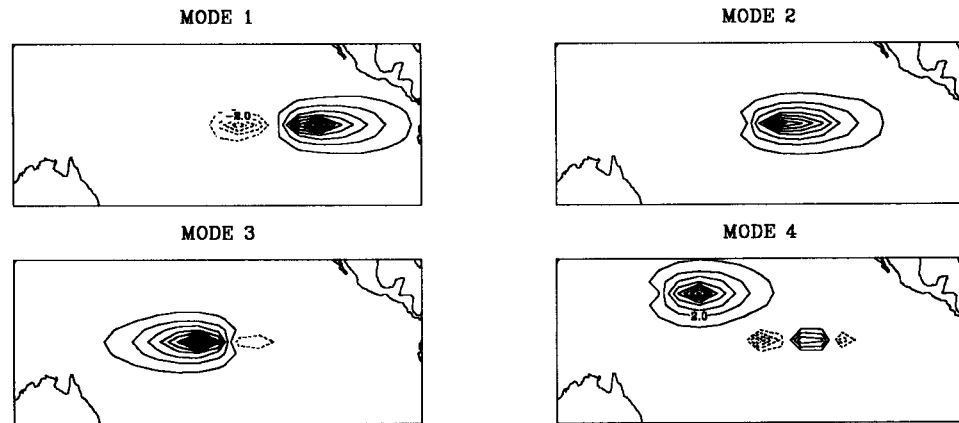


FIG. 7. Four REOF patterns (experiment 3). The EOF modes in Fig. 6 have been simplified by varimax rotation. Much of the dipole and elongated structures of EOFs have been removed but the resulting REOF modes are still much different from the exact physical modes.

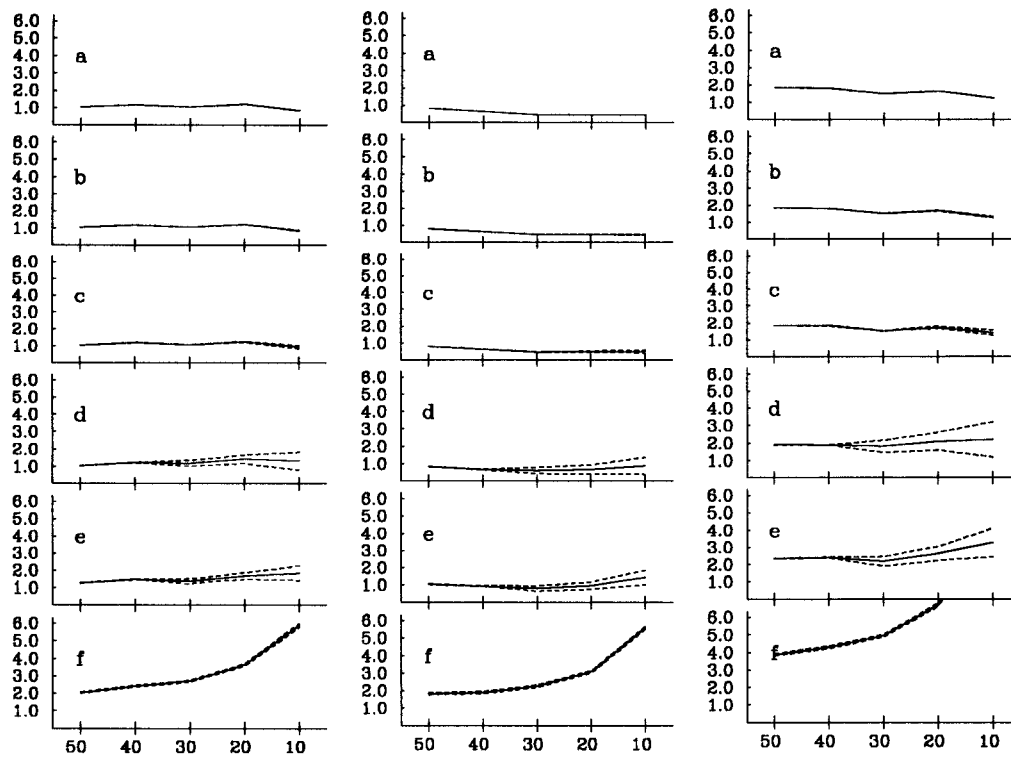


FIG. 8. Ensemble mean and standard deviation of the first eigenvalue (left), the second eigenvalue (middle), and the sum of the two (right) of the first dataset. Standard deviation of sampling error at each grid point is (a) 0.01, (b) 0.05, (c) 0.1, (d) 0.2, (e) 0.5, and (f) 1.0, respectively.

lations increase from 0.05 to 0.53 and 0.51 when the level of background noise is 0.5 [panel (e)]. Even for negligible background noise temporal correlations significantly deteriorate for a short record. For example, correlations are 0.87 and 0.81 and cross correlations are 0.58 and 0.50 for a 10-yr record [panel (a)]. For a sufficiently long record the agreement between the exact PC time series and the estimates is reasonable as long as the level of background noise does not exceed 50% of modal variances.

For the second datasets with moving patterns general sensitivity trends are similar to those of the first datasets with greater error with increased background noise and decreased record length. There is one significant difference between the two, which is worthy of note. Generally, moving patterns are much less sensitive than deforming patterns to the magnitude of background noise and the record length. This is because of the dissimilar nature of signals and noise. Namely, there is little chance that background noise that is stationary (at least in this experiment) is mistaken for moving signals. Therefore, comparisons of eigenvalues and pattern and temporal correlations between the exact modes and the extracted patterns are more favorable for the second dataset than for the first dataset with tighter standard deviations (figures not shown).

## 6. Application to El Niño

EOF techniques are frequently used to derive dominant patterns of ST anomalies associated with El Niño, which together with corresponding PC time series are an important piece of information for El Niño prediction. Figure 11 shows the first two dominant EOF patterns from a tropical Pacific monthly ST dataset (1950–1996) derived from the Comprehensive Ocean–Atmosphere Data Set (Woodruff et al. 1987). The dataset is in  $2^\circ \times 2^\circ$  and represents the sea surface temperature over the ocean and the surface atmospheric temperature over land. They are also reproduced similarly from simulated ST anomalies. Here, a test was carried out to examine how consistent these El Niño patterns are among different eigen techniques. Analysis of ST variance by month also indicates that there is a notable annual cycle in the ST variability (von Storch et al. 1995). Thus, it would be interesting to see if eigen techniques based on the cyclostationarity assumption alter the dominant El Niño patterns in any significant way.

Tables 4 and 5 show cross correlations of the first two dominant ST anomaly patterns. The first pattern is reproduced rather consistently by all of the eigen techniques employed here except for the REOF technique. Pattern correlations are high but modal mixing and splitting are also obvious in the nonnegligible second-best

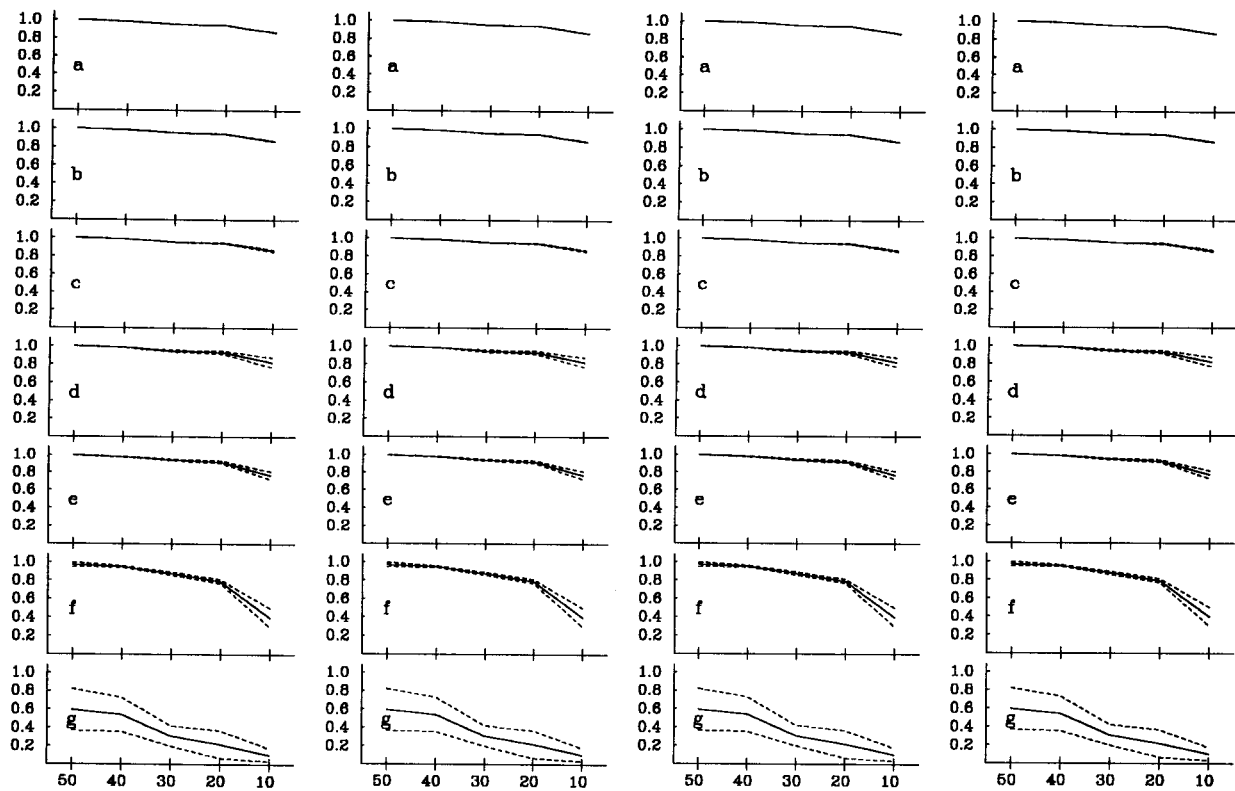


FIG. 9. Mean and standard deviation of the cross pattern correlations between the exact modes and contaminated modes of the first dataset. The correlations are between the first exact mode and the first EOF (first column), first exact mode and second EOF (second column), second exact mode and first EOF (third column), and second exact mode and second EOF (fourth column). Standard deviation of sampling error at each grid point is (a) 0.01, (b) 0.05, (c) 0.1, (d) 0.2, (e) 0.5, (f) 1.0, and (g) 2.0, respectively.

correlations. The POP and CSPOP methods identify several modes that are similar to the first EOF pattern.

The first REOF is somewhat different from the rest of the derived patterns. It is impossible to exclude the possibility that the REOF is most accurate. It was found from previous experiments, however, that the rotation of EOFs does not necessarily lead to more accurate patterns, particularly for nonstationary patterns. While previous studies report greater stability and physical realism of rotated patterns, this study reports the extreme sensitivity of the REOF technique. Rotated patterns were very sensitive to the number of EOF patterns retained for rotation, normalization of the EOF patterns, and the domain size.

The second pattern is not consistent among different techniques. It is rather difficult to say which one is most accurate. According to the pattern correlations, however, EOF, REOF, CEOF, EXEOF, and CSEOF produce patterns that are similar (correlation >0.8) to each other. Except for the CSEOF pattern, second-best correlation is also high for these techniques thereby indicating significant modal mixing and splitting.

Temporal correlations show similar patterns (table not shown). The PC time series of the first mode are generally highly correlated with each other. Again, modal mixing and splitting is obvious for EXEOF, PXEOF,

POP, and CSPOP. The PC time series of the second mode are generally not consistent with each other. The temporal correlations are less than 0.8 except between the EOF and CSEOF techniques. Even with high temporal correlation PC time series from the latter two techniques are different in detail. The PC time series derived from a stationary technique is typically more wiggly than that from a cyclostationary counterpart (Fig. 12). This is because a former technique cannot resolve temporal variations of eigenfunctions. This may bear an important implication on the prediction of El Niño using patterns derived from eigen techniques.

Despite the encouraging results in earlier experiments, the performance of the PXEOF technique is poor for the actual dataset. This may be because of significant sampling error associated with the short record length. The actual dataset is more variable with more noise than those in the synthetic experiments earlier, and accurate statistics could not be obtained from a relatively short record. Typically, the situation is less favorable for the PXEOF technique because the length of each segment in (13) is only a fraction of the total record length, and is therefore more susceptible to sampling error.

Finally, it should be examined if the poor consistency in Tables 5 and 6 represents essential discordance of different eigen techniques or simply sampling errors or

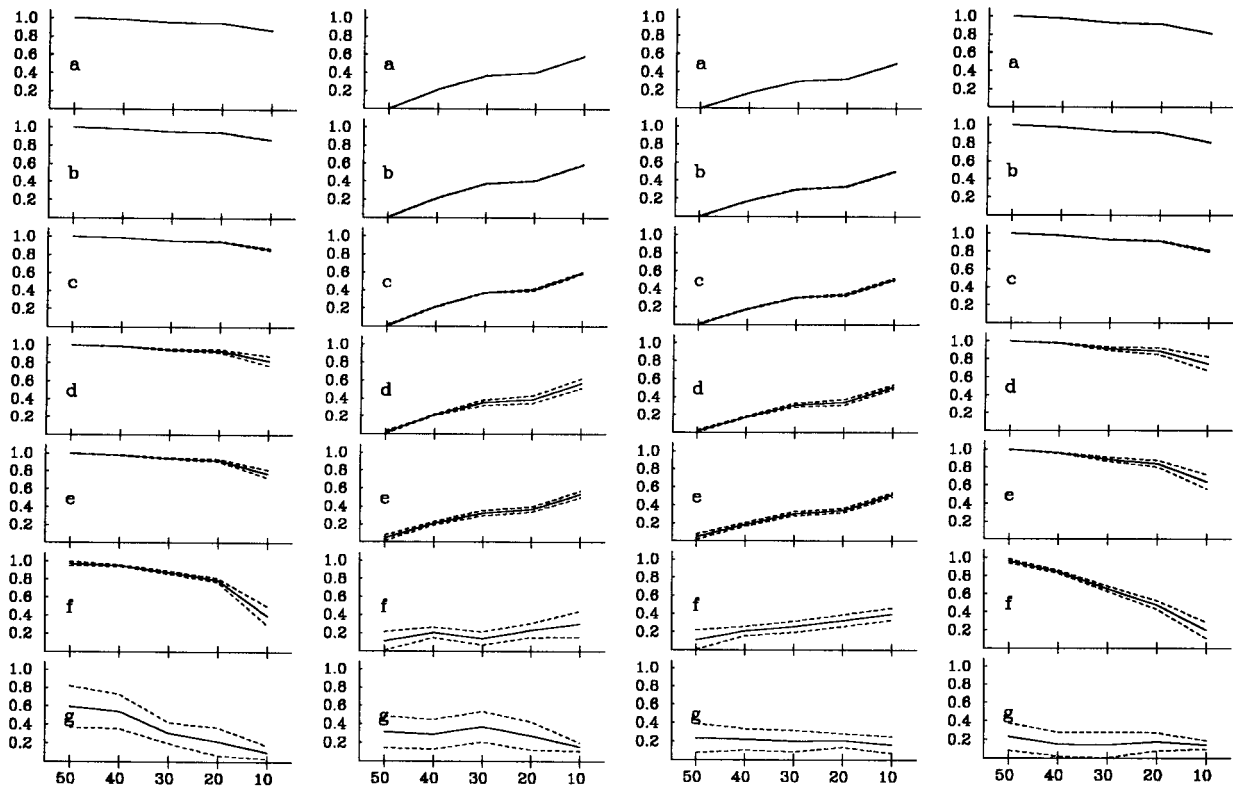


FIG. 10. Mean and standard deviation of the cross correlations between the PC time series of exact modes and those of contaminated modes of the first dataset. The correlations are between the first exact mode and the first EOF (first column), first exact mode and second EOF (second column), second exact mode and first EOF (third column), and second exact mode and second EOF (fourth column). Standard deviation of sampling error at each grid point is (a) 0.01, (b) 0.05, (c) 0.1, (d) 0.2, (e) 0.5, (f) 1.0, and (g) 2.0, respectively.

weakness of the modes compared with background noise. Therefore, let us examine how sensitive CSEOFs are to the record length. Table 6 shows pattern and temporal correlations between the CSEOFs of the full dataset (1950–1996) and estimates based on differing lengths of the dataset. Note that the first two modes are well shielded from sampling noise as indicated by fairly

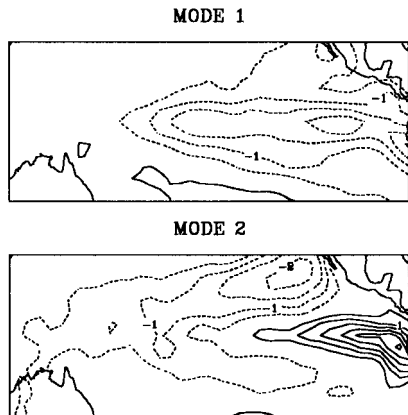


FIG. 11. Two dominant patterns of tropical Pacific ST anomaly field (1950–1996).

high correlations, even for a short record length (see also Figs. 9 and 10). Also small cross-correlations imply only a little mixing and indicates that the two eigenvalues are well separated compared with the noise level.

The concordance of the major patterns and the corresponding PC time series in Table 6 for a 40-yr record with those of the full dataset is much better than the consistency among different eigen techniques in Tables 4 and 5. Although a conclusive statement is difficult to make from the limited experiment included here, it seems like the discordance in Tables 4 and 5 is not entirely due to sampling error or background noise but rather reflects essential difference among different eigen techniques.

## 7. Summary and concluding remarks

While EOF patterns and corresponding PC time series constitute important information for climate studies, they may vary depending upon the particular eigen technique employed. Considered in this study was a comparison of eight eigen techniques as to their ability to reproduce physical/dynamical patterns faithfully from a dataset. These eigen techniques were applied, in particular, to nonstationary datasets with periodic statistics.



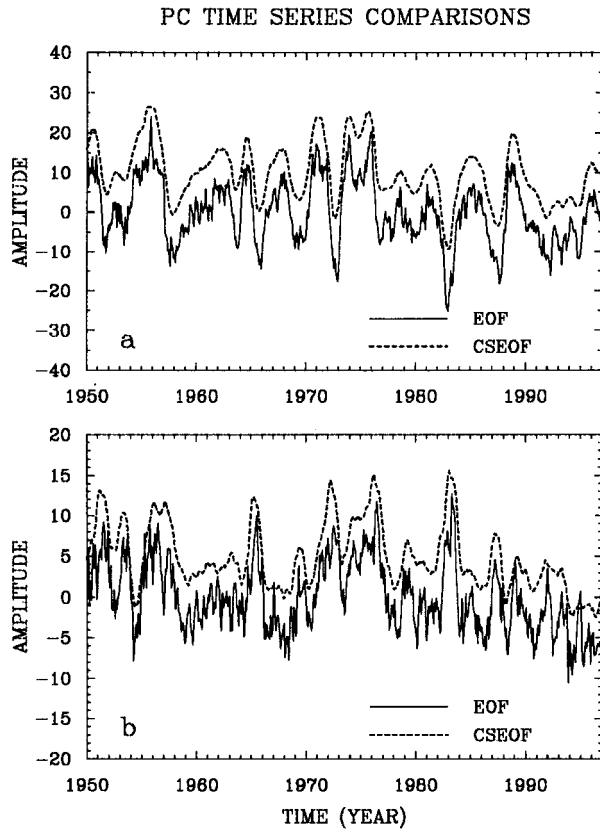


FIG. 12. Comparisons of the first two dominant PC time series of tropical Pacific ST (1950–96) derived from the EOF and CSEOF techniques: (a) first mode and (b) second mode. The CSEOF time series were shifted upward for easy comparison. Because the stationary technique (EOF) does not resolve the temporal evolution of physical modes, the corresponding PC time series are more erroneously estimated than the cyclostationary counterpart

dataset. Thus, discretion should be exercised as to the adequacy of this technique for each dataset.

Finally, eigen techniques were applied to the ST of the tropical Pacific to identify patterns associated with El Niño. The pattern correlations are high for the first mode except for the REOF. The REOF mode is not very

consistent with the rest of the derived patterns. There is some hint of modal mixing and splitting for the CEOF, EXEOF, PXEOF, POP, and CSPOP techniques. The second modes, however, are not very consistent among different techniques. Only EOF, REOF, CEOF, EXEOF, and CSEOF produce similar modes with high pattern correlations (>0.8). Of these, only EOF and CSEOF produce similar PC time series with correlation greater than 0.8. This indicates that the seasonal cycle in the statistics of the tropical Pacific ST is moderately small. A limited sensitivity test seems to indicate that the discordance among eigen techniques mainly reflect material difference among different eigen techniques, not just sampling error or the weakness of the extracted modes. Even with a relatively high correlation there is a detailed difference between the two PC time series. Specifically, eigen techniques based on the stationarity assumption produce PC time series that are more wiggly than a cyclostationary counterpart. This is due to their inability to resolve the evolving patterns of a dataset. Thus, the resolution of cyclic statistics may be an important consideration and may improve the predictability of El Niño.

*Acknowledgments.* We thank the National Science Foundation for its support of this work via Grant ATM-9613748 to Texas A&M University.

REFERENCES

Barnett, T. P., 1983: Interaction of the Monsoon and Pacific trade wind system at interannual time scales. Part I. The equatorial zone. *Mon. Wea. Rev.*, **111**, 756–773.  
 —, 1985: Variations in near-global sea level pressure. *J. Atmos. Sci.*, **42**, 478–501.  
 —, M. Latif, N. Graham, M. Flügel, S. Pazan, and W. White, 1993: ENSO and ENSO-related predictability. Part I: Prediction of equatorial Pacific sea surface temperature with a hybrid coupled ocean–atmosphere model. *J. Climate*, **6**, 1545–1566.  
 Barnston, A. G., and R. E. Livezey, 1987: Classification, seasonality and persistence of low-frequency atmospheric circulation patterns. *Mon. Wea. Rev.*, **115**, 1083–1126.  
 Blumenthal, M. B., 1991: Predictability of a coupled ocean–atmosphere model. *J. Climate*, **4**, 766–784.

TABLE 6. Spatial and temporal correlations of the first three dominant CSEOF patterns and the corresponding principal component time series based on the full dataset with those of employing different lengths of data. The dataset is a monthly tropical Pacific surface temperature anomaly field (1950–96). Each block consists of two lines of entries: best and second-best pattern correlations with mode numbers in parenthesis (first line), and best and second-best temporal correlations (second line).

Case (yr)	Mode 1		Mode 2		Mode 3	
40	1.00 (1)	0.02 (7)	0.99 (2)	0.05 (7)	0.99 (3)	0.06 (5)
	1.00 (1)	0.08 (7)	1.00 (2)	0.09 (4)	0.99 (3)	0.06 (5)
30	0.98 (1)	0.07 (5)	0.93 (2)	0.16 (3)	0.83 (3)	0.21 (2)
	1.00 (1)	0.15 (5)	0.95 (2)	0.23 (5)	0.89 (3)	0.21 (10)
20	0.92 (1)	0.09 (5)	0.81 (2)	0.17 (5)	0.70 (3)	0.35 (4)
	0.99 (1)	0.23 (3)	0.90 (2)	0.29 (5)	0.77 (3)	0.43 (4)
10	0.86 (1)	0.08 (4)	0.69 (2)	0.21 (3)	0.46 (4)	0.34 (3)
	0.97 (1)	0.23 (4)	0.81 (2)	0.33 (3)	0.59 (4)	0.39 (3)

- Braconnot, P., and C. Frankignoul, 1993: Testing model simulations of the thermocline depth variability in the tropical Atlantic from 1982 through 1984. *J. Phys. Oceanogr.*, **23**, 626–647.
- Buell, C. E., 1975: The topography of empirical orthogonal functions. Preprints, *Fourth Conf. on Probability and Statistics in Atmospheric Sciences*, Tallahassee, FL, Amer. Meteor. Soc., 188–193.
- , 1979: On the physical interpretation of empirical orthogonal functions. Preprints, *Sixth Conf. on Probability and Statistics in Atmospheric Sciences*, Banff, AB, Canada, Amer. Meteor. Soc., 112–117.
- Bürger, G., 1993: Complex principal oscillation patterns. *J. Climate*, **6**, 1972–1986.
- Chen, D., S. E. Zebiak, A. J. Busalacchi, M. A. Cane, 1995: An improved procedure for El Niño forecasting: Implications for predictability. *Science*, **269**, 1699–1702.
- Cheng, X., G. Nitsche, and J. M. Wallace, 1995: Robustness of low-frequency circulation patterns derived from EOF and rotated EOF analyses. *J. Climate*, **8**, 1709–1713.
- Davey, M. K., D. L. T. Anderson, and S. Lawrence, 1996: A simulation of variability of ENSO forecast skill. *J. Climate*, **9**, 240–246.
- Dunkerton, T. J., 1993: Observation of 3–6-day meridional wind oscillations over the tropical Pacific, 1973–1992: Vertical structure and interannual variability. *J. Atmos. Sci.*, **50**, 3292–3307.
- Graham, N. E., J. Bichaelsen, and T. P. Barnett, 1987a: An investigation of the El Niño–Southern Oscillation cycle with statistical models. 1. Predictor field characteristics. *J. Geophys. Res.*, **92**, 14 251–14 270.
- , —, and —, 1987b: An investigation of the El Niño–Southern Oscillation cycle with statistical models. 2. Model results. *J. Geophys. Res.*, **92**, 14 271–14 289.
- Hasselmann, K., 1988: PIPs and POPs: The reduction of complex dynamical systems using principal interaction and oscillation patterns. *J. Geophys. Res.*, **93**, 11 015–11 021.
- , 1993: Optimal fingerprints for the detection of time-dependent climate change. *J. Climate*, **6**, 1957–1971.
- Hegerl, G. C., H. von Storch, K. Hasselmann, B. D. Santer, U. Cubasch, and P. D. Jones, 1996: Detecting greenhouse-gas-induced climate change with an optimal fingerprint method. *J. Climate*, **9**, 2281–2306.
- Horel, J. D., 1984: Complex principal component analysis: Theory and examples. *J. Climate Appl. Meteor.*, **23**, 1660–1673.
- Kim, K.-Y., 1997: Statistical interpolation using cyclostationary EOFs. *J. Climate*, **10**, 2931–2942.
- , and G. R. North, 1997: EOFs of harmonizable cyclostationary processes. *J. Atmos. Sci.*, **54**, 2416–2427.
- , —, and J. Huang, 1996a: EOFs of one-dimensional cyclostationary time series: Computations, examples, and stochastic modeling. *J. Atmos. Sci.*, **53**, 1007–1017.
- , —, and S. S. Shen, 1996b: Optimal estimation of spherical harmonic components from a sample with spatially nonuniform covariance statistics. *J. Climate*, **9**, 635–645.
- Latif, M., and M. Flügel, 1991: An investigation of short range climate predictability in the tropical Pacific. *J. Geophys. Res.*, **96**, 2661–2673.
- , A. Sterl, E. Maier-Reimer, and M. M. Junge, 1993: Climate variability in a coupled GCM. Part I: The tropical Pacific. *J. Climate*, **6**, 5–21.
- Lau, K.-M., and P. H. Chan, 1985: Aspects of the 40–50 day oscillation during the northern winter as inferred from outgoing longwave radiation. *Mon. Wea. Rev.*, **113**, 1889–1909.
- Montroy, D. L., 1997: Linear relation of central and eastern North American precipitation to tropical Pacific sea surface temperature anomalies. *J. Climate*, **10**, 541–558.
- North, G. R., 1984: Empirical orthogonal functions and normal modes. *J. Atmos. Sci.*, **41**, 7563–7571.
- , and R. F. Cahalan, 1981: Predictability in a solvable stochastic climate model. *J. Atmos. Sci.*, **38**, 504–513.
- , and K.-Y. Kim, 1995: Detection of forced climate signals. Part II: Simulation results. *J. Climate*, **8**, 409–417.
- , —, S. S. Shen, and J. W. Hardin, 1995: Detection of forced climate signals. Part I: Filter theory. *J. Climate*, **8**, 401–408.
- Penland, C., and T. Magorian, 1993: Prediction of Niño 3 sea surface temperatures using linear inverse modeling. *J. Climate*, **6**, 1067–1067.
- Plaut, G., and R. Vautard, 1994: Spells of low-frequency oscillations and weather regimes over the Northern Hemisphere. *J. Atmos. Sci.*, **51**, 210–236.
- Richman, M. B., 1986: Rotation of principal components. *J. Climatol.*, **6**, 293–335.
- Santer, B. D., W. Brüggerman, U. Cubasch, K. Hasselmann, H. Höck, E. Maier-Reimer, and U. Mikolajewicz, 1994: Signal-to-noise analysis of time-dependent greenhouse warming experiments. *Climate Dyn.*, **9**, 267–285.
- Schnur, R., G. Schmitz, N. Grieger, and H. von Storch, 1993: Normal modes of the atmosphere as estimated by principal oscillation patterns and derived from quasigeostrophic theory. *J. Atmos. Sci.*, **50**, 2386–2400.
- Shen, S. S., G. R. North, and K.-Y. Kim, 1994: Spectral approach to optimal estimation of the global average temperature anomaly. *J. Climate*, **7**, 1997–2007.
- von Storch, H., G. Bürger, R. Schnur, and J.-S. von Storch, 1995: Principal oscillation patterns: A review. *J. Climate*, **8**, 377–400.
- Wallace, J. M., and R. E. Dickinson, 1972: Empirical orthogonal representation of time series in the frequency domain. Part I: Theoretical considerations. *J. Appl. Meteor.*, **11**, 887–892.
- Weare, B. C., and J. N. Nasstrom, 1982: Examples of extended empirical orthogonal function analyses. *Mon. Wea. Rev.*, **110**, 481–485.
- Woodruff, S. D., R. J. Sultz, R. L. Jenne, and P. M. Steurer, 1987: A Comprehensive Ocean–Atmosphere Data Set. *Bull. Amer. Meteor. Soc.*, **68**, 1239–1250.
- Xu, J.-S., 1993: The joint modes of the coupled atmosphere–ocean system observed from 1967 to 1986. *J. Climate*, **6**, 816–838.
- , and H. von Storch, 1990: Predicting the state of the Southern Oscillation using principal oscillation pattern analysis. *J. Climate*, **3**, 1316–1329.
- Zwiers, F. W., 1993: Simulation of the Asian monsoon with the CCC GCM-1. *J. Climate*, **6**, 470–486.